A&A 528, A63 (2011)
DOI: 10.1051/0004-6361/201015764

Astronomy & Astrophysics

SOPHIE velocimetry of *Kepler* transit candidates⋆

II. KOI-428b: a hot Jupiter transiting a subgiant F-star

A. Santerne[1,3], R. F. Díaz[2,3], F. Bouchy[2,3], M. Deleuil[1], C. Moutou[1], G. Hébrard[2,3], A. Eggenberger[4], D. Ehrenreich[4], C. Gry[1], and S. Udry[5]

[1] Laboratoire d'Astrophysique de Marseille, Université d'Aix-Marseille & CNRS, 38 rue Frédéric Joliot-Curie, 13388 Marseille Cedex 13, France
e-mail: alexandre.santerne@oamp.fr
[2] Institut d'Astrophysique de Paris, UMR7095 CNRS, Université Pierre & Marie Curie, 98bis boulevard Arago, 75014 Paris, France
[3] Observatoire de Haute Provence, Université d'Aix-Marseille & CNRS, 04670 Saint Michel l'Observatoire, France
[4] Laboratoire d'Astrophysique de Grenoble, Université Joseph Fourier, CNRS (UMR 5571), BP 53, 38041 Grenoble Cedex 9, France
[5] Observatoire de Genève, Université de Genève, 51 Ch. des Maillettes, 1290 Sauverny, Switzerland

Received 15 September 2010 / Accepted 31 December 2010

ABSTRACT

We report the discovery of a hot Jupiter transiting a subgiant star with an orbital period of 6.87 days. This discovery was aided by public photometric data from the *Kepler* space mission and new radial velocity observations obtained by the SOPHIE spectrograph. The planet KOI-428b, with a radius of $1.17 \pm 0.04\ R_{\rm Jup}$ and a mass of $2.2 \pm 0.4\ M_{\rm Jup}$, orbits an F5IV star with $R_\star = 2.13 \pm 0.06\ R_\odot$, $M_\star = 1.48 \pm 0.06\ M_\odot$, and $T_{\rm eff} = 6510 \pm 100$ K. The star KOI-428 is the largest and the most evolved star discovered so far with a transiting planet.

Key words. techniques: spectroscopic – techniques: radial velocities – techniques: photometric – planetary systems – stars: individual: KOI-428b

1. Introduction

After its launch in March 2009, *Kepler* became the second space mission designed to find transiting exoplanets with high-accuracy photometry. This mission has already shown its ability to discover new planets during the first 33.5 days of science operations with the announcement of a hot-Neptune-like planet (Borucki et al. 2010a), four hot-Jupiters (Koch et al. 2010; Jenkins et al. 2010a; Dunham et al. 2010; Latham et al. 2010), a system of two transiting Saturns (Holman et al. 2010) and a transiting rocky planet (Batalha et al. 2011). From the 156 000 stars observed, 706 exoplanet candidates were identified, with 306 of them were published by Borucki et al. (2010b). All these candidates have been detected around faint stars ($14 \leq m_{\rm V} \leq 16$) not included in the ground-based follow-up conducted by the Kepler team.

To establish the planetary nature of these candidates and to assess the fraction of false positives, a high-resolution spectroscopic follow-up must be carried out. This could allow various configurations of eclipsing binaries to be discarded and the properties (mass, density) of actual planets to be established (Bouchy et al. 2009b). We present here the radial velocity follow-up performed with the SOPHIE spectrograph, which is mounted on the 1.93-m telescope at the Observatoire de Haute Provence, of the Kepler Object of Interest KOI-428. It was observed as part of a first set of *Kepler* targets followed up with SOPHIE (Bouchy et al., in prep.). This led to the discovery and characterization of the new exoplanet KOI-428b.

⋆ Based on observations made with the 1.93-m telescope at Observatoire de Haute-Provence (CNRS), France.

2. *Kepler* observations

The target KOI-428 was observed by *Kepler* during the first 33.5-day segment of the science operations (Q1) from May 13 to June 15, 2009 with a temporal sampling of 29.4 min. The various identifications of this target, including coordinates and magnitudes, are listed in Table 1. The publicly-available[1] *Kepler* light curve contains1639 points, thirteen of which are affected by known systematic effects, such as the loss of fine pointing caused by momentum desaturation or the occurrence of strong argabrightenings[2], and were discarded by the *Kepler* pipeline (Jenkins et al. 2010b). Based on the four transits that occurred during Q1, Borucki et al. (2010b) report that this system consists of a ∼1.93 solar radius star with a 1.04 Jupiter radius companion in a 6.87-day orbit. Figure 1 presents the corrected light curve from the MAST database showing four periodic transit events with a depth of about 3.9 mmag. One can see from this figure that the first event is slightly deeper than the other three. We therefore studied whether other known systematic effects were present during the transits, in particular during the first one. We found that none of the transits were affected by reaction wheel zero crossings or by fainter argabrightenings, which were not discarded by the pipeline. Also, no difference was observed in the out-of-transit flux of the first transit as compared to the other

[1] http://archive.stsci.edu/kepler/data_search/search.php

[2] Name given to cadences for which all the focal plane is illuminated by a presently unexplained effect. For more informations, see http://archive.stsci.edu/kepler/release_notes/release_notes5/Data_Release_05_2010060414.pdf, Sect. 6.1.

Table 1. KOI428 IDs, coordinates and magnitudes.

Kepler input catalog (KIC)	10418224
Kepler object of interest (KOI)	428.01
2MASS ID	19471528+4731357
Right Ascension (J2000)	19:47:15.29
Declinaison (J2000)	+47:31:35.8
Kepler magnitude[a]	14.58 ± 0.02
B^b	14.9
R^b	14.3
J^c	13.536 ± 0.021
H^c	13.294 ± 0.022
K^c	13.27 ± 0.30
$E(B-V)^a$	0.139 ± 0.1

Notes. [(a)] From the Kepler Input Catalog. [(b)] From USNO-A2 catalog. [(c)] From 2MASS catalog.

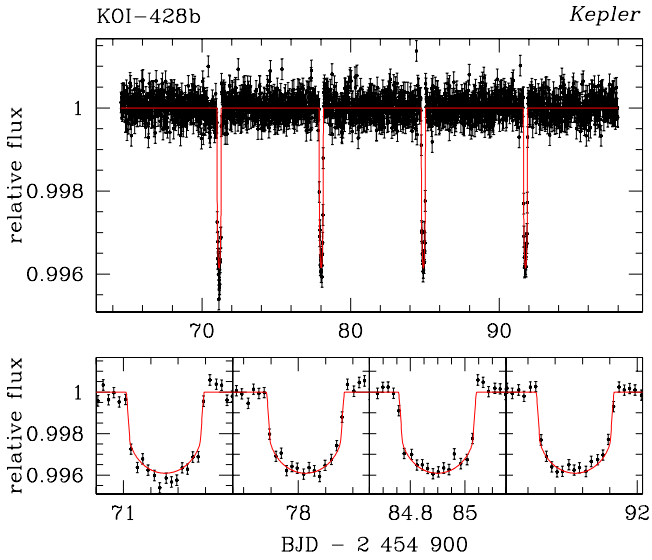

Fig. 1. Light curve available on MAST database showing the four transits detected on KOI-428. The red curve shows the best fit of the transit.

three, which would have indicated that the difference in depth of the first transit was caused by the detrending performed by the pipeline. On the other hand, it is known that during Q0 and Q1 a couple of variable stars – an eclipsing binary and an intrinsic variable – were chosen as guide stars and that this affected the spacecraft guiding. As a consequence, the time series of the column position of KOI428 presents positive, sharp, transit-like features lasting about 10–15 cadences. One of these "bumps" coincides with the first transit and might explain the amplitude difference observed. Since the inclusion of this transit in our fitting procedure does not change our results significantly, we decided to use the whole *Kepler* light curve as provided in the MAST database.

3. SOPHIE observations

We performed the high-resolution spectroscopy follow-up of KOI-428 as part of a first set of *Kepler* candidates (Bouchy et al., in prep.) with the SOPHIE spectrograph (Perruchot et al. 2008; Bouchy et al. 2009a) installed on the 1.93 m telescope at the Observatoire de Haute-Provence, France. SOPHIE is a cross-dispersed, high-resolution, fiber-fed echelle spectrograph, stabilized in pressure and temperature and calibrated with a thorium-argon lamp, mainly dedicated to measure precise radial

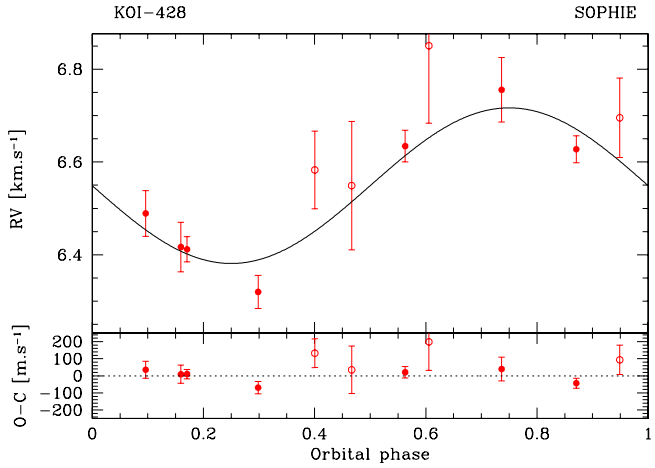

Fig. 2. Phase-folded radial velocity curve with our best fit (*top panel*) and residuals (*bottom panel*). Open circles represent the four observations strongly affected by the scattered Moon light.

velocity (RV) on solar-type stars for exoplanets and asteroseismology studies.

Observations were made with the high-efficiency mode, with a spectral resolution of 39 000 at 550 nm and the slow read-out CCD mode. Our observations made use of both of the SOPHIE fibers : fiber A was centered on the target, while fiber B acquired the sky background ∼2 arcmin from the target. The typical intrinsic stability of SOPHIE (3 $\mathrm{m\,s^{-1}h^{-1}}$) does not require using the simultaneous calibration, and the sky fiber is critical for removinf the scattered Moon light. Eleven spectra of KOI-428 were obtained from July 15 to September 13, 2010 with an exposure time of 1 h. SOPHIE spectra were reduced with the online pipeline. Radial velocities were obtained by computing the weighted cross-correlation function (CCF) of the spectra using a numerical spectral mask corresponding to a G2V star (Baranne et al. 1996; Pepe et al. 2002). Four spectra were strongly affected by the Moon's background light and were corrected with the same procedure as for previous planets (Pollacco et al. 2008; Barge et al. 2008; Hébrard et al. 2008) and as described for *HARPS* (Bonomo et al. 2010). This effect cannot be removed completely on such a faint star, so we conservatively doubled the uncertainties of the four corresponding measurements to account for possibly remaining systematics and to get a reduced χ^2 close to one. Radial velocities are listed in Table 3 and plotted in Fig. 2. They show a clear variation in phase with the *Kepler* ephemeris listed in Table 2 and compatible with the reflex motion of the parent star due to a planetary companion. Since no significant eccentricity is seen in the data ($e = 0.05 \pm 0.21$) we decided to fit a Keplerian circular orbit using the updated ephemeris listed in Table 2. This does not affect the radial velocity semi-amplitude within 1-σ level. The best fit has semi-amplitude $K = 179 \pm 27$ $\mathrm{m\,s^{-1}}$ and a $\sigma_{\mathrm{O-C}} = 65$ $\mathrm{m\,s^{-1}}$ which is comparable to the mean radial velocity uncertainty.

To assess the possibility that the RV variations stem from to a blended binary, we checked both the variations in the bisector span of the CCF and the dependences of the RV variations with different cross-correlation masks (Bouchy et al. 2009b). The CCFs were computed with F0V, G2V, and K5V masks for all the spectra, and no significant differences were found in the amplitude of the RV variations ($K_{F0V} = 177 \pm 44\,\mathrm{m\,s^{-1}}$, $K_{G2V} = 179 \pm 27\,\mathrm{m\,s^{-1}}$, $K_{K5V} = 194 \pm 32\,\mathrm{m\,s^{-1}}$). The bisector span, listed in Table 3 and plotted in Fig. 3, does not reveal any significant variations at a level more than two times smaller than the RV changes. Moreover, neither radial velocities,

Table 2. Star and planet parameters.

Ephemeris	
Planet orbital period P [days]	6.87349 ± 0.00064
Transit epoch $T_{\rm tr}$ [BJD]	$2\,455\,005.5198 \pm 0.0024$
Results from radial velocity observations	
Orbital eccentricity e	0 (fixed)
Semi-amplitude K [m s^{-1}]	179 ± 27
Systemic velocity V_r [km s^{-1}]	6.565 ± 0.020
O–C residuals [m s^{-1}]	65
Fitted transit parameters	
Radius ratio $k = R_{\rm p}/R_\star$	0.0565 ± 0.0004
Scaled semi-major axis $a/R_\star$	8.11 ± 0.06
Impact parameter b	$0.045^{+0.011}_{-0.037}$
Deduced transit parameters	
$M_\star^{1/3}/R_\star$[solar units]	0.533 ± 0.004
Stellar density $\rho_\star$ [g cm^{-3}]	0.213 ± 0.005
Inclination I [deg]	$89.7^{+0.3}_{-0.1}$
Transit duration T_{14} [h]	6.86 ± 0.06
Spectroscopic parameters	
Effective temperature $T_{\rm eff}$ [K]	6510 ± 100
Metallicity [Fe/H] [dex]	$0.10^{+0.15}_{-0.10}$
Stellar rotational velocity $\upsilon \sin i$ [km s^{-1}]	9.0 ± 2
Spectral type	F5IV
Stellar and planetary physical parameters from combined analysis	
Star mass $M_\star$ [$M_\odot$]	1.48 ± 0.06
Star radius $R_\star$[$R_\odot$]	2.13 ± 0.06
Surface gravity $\log g^a$ [dex]	3.94 ± 0.32
Age of the star t [Gy]	2.8 ± 0.3
Distance of the system [pc]	2700 ± 200
Orbital semi-major axis a^b [AU]	0.080 ± 0.003
Planet mass $M_{\rm p}$ [M_J]	2.2 ± 0.4
Planet radius $R_{\rm p}$[R_J]	1.17 ± 0.04
Planet density $\rho_{\rm p}$ [g cm^{-3}]	$1.68^{+0.53}_{-0.43}$
Equilibrium temperature ^{c} $T_{\rm eq}$ [K]	1620 ± 30

Notes. $^{(a)}$ Derived from $M_\star$ and $R_\star$. $^{(b)}$ Derived from $a/R_\star$ and $R_\star$. $^{(c)}$ Considering a zero albedo and a perfect atmospheric thermal circulation.

nor their residuals present any significant correlation with the bisector (We find a Spearman's rank-order correlation coefficient between RV and bissector of -0.17 ± 0.31). These tests allow us to secure the planetary nature of KOI-428b.

4. Spectral classification

We performed the spectroscopic analysis of the parent star KOI-428 using SOPHIE spectra. Individual spectra have a low signal-to-noise, which does not allow a proper spectral analysis. Therefore, we co-added order per order the first 5 spectra not affected by the Moon light once set to the barycentric rest frame. We finally get a co-added spectrum with an $S/N \approx 82$ per element of resolution on the continuum at 5550 Å with a spectral resolution of 39 000. We derived the star's photospheric parameters using the semi-automatic software package VWA (Bruntt et al. 2002, 2008) as described in Bruntt et al. (2010). We derived $\upsilon \sin i = 9.0 \pm 2$ km s^{-1}, $\upsilon_{\rm micro} = 1.0 \pm 1$ km s^{-1}, $T_{\rm eff} = 6510 \pm 100$ K, and [Fe/H] $= 0.1^{+0.15}_{-0.1}$. We estimated the surface gravity by fitting synthetic spectra to the wings of the Mg I b and Na I D lines and adopting the abundances derived from weak lines. We found $\log g = 4.1 \pm 0.2$, a value that the quite low S/N combined to the moderate spectral resolution did not allow us to accurately estimate. The derived stellar parameters are reported in Table 2. Our stellar parameters are significantly different from those given by Borucki et al. (2010b) ($T_{\rm eff} = 6127$ K and $\log g = 4.55$). However, these authors note that "spectroscopic observations have not been made for the released stars, so it is important to recognize that some of the characteristics listed for the stars are uncertain, especially surface gravity". Using Eq. (3) in Casagrande et al. (2010) with the J and K magnitudes from the 2MASS archive (listed in Table 1) and a reddening $E(J-K) = 0.074$ (computed from Cardelli et al. 1989), we computed a photometric temperature $T_{\rm eff} = 6604 \pm 132$ K, which is in good agreement with the spectroscopic value.

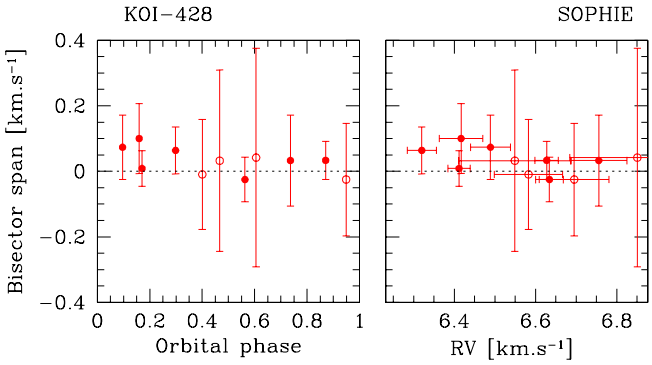

Fig. 3. Bisector variations as function of the orbital phase (*left panel*) and as function of radial velocity (*right panel*). Open circles display the four observations affected by the background Moon light. Bisector error bars are taken as twice the radial velocity uncertainties. No significant slope is visible between radial velocity and bisector, discarding a blend scenario.

Table 3. SOPHIE measurements of KOI-428.

BJD (−2 455 000)	RV [km s^{-1}]	$\pm 1\sigma_{rv}$ [km s^{-1}]	BIS [km s^{-1}]	S/N/pix @550 nm
392.5085	6.320	0.036	0.064	15.7
395.5188	6.755	0.069	0.033	10.2
396.4422	6.627	0.029	0.033	20.2
398.5034	6.411	0.027	0.009	21.0
400.5389^a	6.549	0.138	0.032	12.0
401.4932^a	6.850	0.166	0.042	10.9
425.4872	6.489	0.049	0.073	12.0
431.3489^a	6.695	0.086	-0.025	18.3
441.3261^a	6.582	0.084	-0.009	15.8
442.4435	6.634	0.034	-0.025	15.5
453.4184	6.417	0.053	0.100	16.1

Notes. $^{(a)}$ Measurement affected by scattered Moon light.

5. System parameters

The *Kepler* light curve was modeled using the analytical expressions from Mandel & Agol (2002) with a linear limb-darkening law. We adjusted the radius ratio $k = R_{\rm p}/R_\star$, the impact parameter b, the system scale $a/R_\star$, and the ephemerides parameters P and $T_{\rm tr}$. The eccentricity of the orbit was set to zero in the light-curve analysis, since there is no compelling evidence from the radial velocity measurements that the orbit is eccentric. The coefficient of the limb darkening law was not adjusted, but was allowed to vary within the limits defined by the spectral analysis

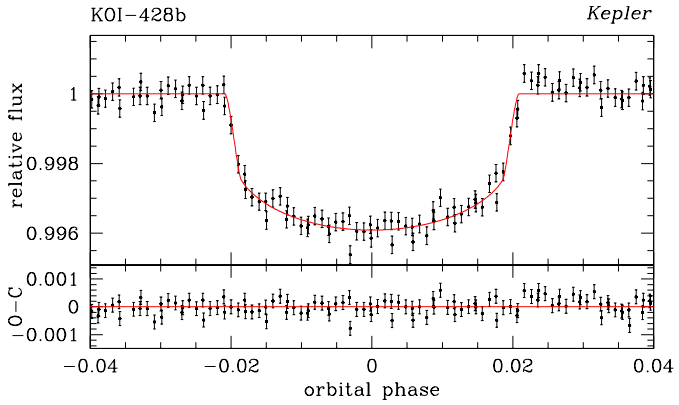

Fig. 4. Unbinned phase-folded light curve and residuals of the four transits of KOI-428 showing the best-fit model of the transit.

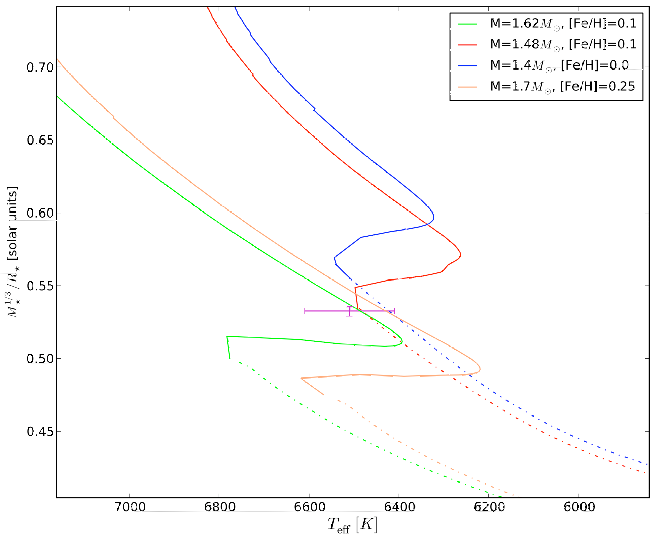

Fig. 5. STAREVOL evolutionary tracks models in the ($T_{\rm eff}$, $M_\star^{1/3}/R_\star$) space for main-sequence stars (solid lines) and post-main sequence stars (dashed-dot lines). The purple point represents the observed position of the star KOI-428 with the associated error bars in this space. The two best models are the green solid line with $M_\star = 1.62\ M_\odot$ and the adopted one in dashed-dot red line with $M_\star = 1.48\ M_\odot$ (see text).

of Sect. 4 (see below). On the other hand, the coarse sampling of the *Kepler* long cadence light curves have been shown to overestimate the impact parameter (Kipping & Bakos 2010) leading to a lower measured stellar density. To avoid this, we followed the solution proposed by Kipping (2010), i.e. we generated an over-sampled model light curve, which we binned to match the sampling rate of the *Kepler* data before comparing it to the actual measurements. For the present analysis our model light curve was five times as densely sampled as the *Kepler* data.

The best-fit parameters were found by χ^2-minimization using the downhill simplex algorithm (Nelder & Mead 1965), as implemented in the SciPy library[3]. The fit was repeated starting from 1500 randomly generated starting points, drawn from uniform distributions that allowed a wide range of values for each parameter. Additionally, the value of the limb-darkening coefficient was drawn at each iteration from a normal distribution centered on the value obtained by linear interpolation of the table by Sing (2010) using the stellar parameters computed with VWA (see Sect. 4), and standard deviation equal to half the difference between the maximum and minimum values allowed by the 1-σ intervals of the stellar parameters. In this way, we try to consider the systematic effects introduced by fixing this value during the fit. The best-fit model is shown in Figs. 1 and 4, and the parameters are listed in Table 2. We also repeated the fit leaving out the first transit, which is slightly deeper than the other three (see Sect. 2). We found that k is within the 1.2-σ, and the other parameters are all within 1-σ of the values determined using the entire dataset.

To estimate the uncertainties in the obtained parameters, we constructed synthetic data sets by scrambling the residuals of the best-fit model and adding them back into the model light curve. We repeated the processes 2000 times, refitting the data for each realization and recording the obtained parameters. Here again, the starting points were randomly varied and the limb-darkening coefficient was drawn from the same distribution. If we assume that the set of transit parameters obtained this way is a good approximation of the true distribution of the best-fit parameters obtained with the downhill simplex algorithm, then we can use it to estimate the confidence intervals of these best-fit parameters. The error bars reported in Table 2 correspond to the 68% confidence interval, defined so that the cumulative probability is 16% above and below the upper and lower confidence limit, respectively.

Finally, the stellar density obtained from the transit fit was used to calculate the value of the surface gravity (see below), which provided a new value for u from which we computed a new value for the stellar density by repeating the whole fitting process. This procedure was iterated until convergence was reached, for $u = 0.548^{+0.015}_{-0.010}$ and the values reported in Table 2.

We used the photospheric parameters from the spectral analysis and the stellar density from the transit modeling to determine the star's fundamental parameters in the ($T_{\rm eff}$, $M_\star^{1/3}/R_\star$) space. The location of the star in the H-R diagram was compared to *STAREVOL* evolution tracks (Palacios, private com.; Turck-Chièze et al. 2010) minimizing the usual χ^2 statistics, but taking the time, τ [Gy], into account that a given model spends in the error box:

$$\chi^2_{\rm model} = \frac{1}{\tau}\left(\frac{T_{\rm eff} - T_{\rm eff,\,model}}{\sigma_{T_{\rm eff}}}\right)^2 + \frac{1}{\tau}\left(\frac{M_\star^{1/3}/R_\star - M_\star^{1/3}/R_{\star\,\rm model}}{\sigma_{M_\star^{1/3}/R_\star}}\right)^2 + \frac{1}{\tau}\left(\frac{\rm [Fe/H]\ - [Fe/H]_{\ model}}{\sigma_{\rm [Fe/H]}}\right)^2.$$

We found two distincts sets of solutions that correspond to different evolutionary states: either the star is in the last main-sequence evolution stage or it is in the very beginning of the post main-sequence phase. The main-sequence solutions correspond to a star with mass of $M_\star = 1.62 \pm 0.10\ M_\odot$, which is close to the red hook at main-sequence turnoff. A similar situation is reported for another planet host star, Kepler-4 (Borucki et al. 2010b), whose location in the H-R diagram is also compatible with the two evolutionary phases that could not be distinguished. In the case of KOI-428, the post main sequence solutions are clearly separated from main sequence solutions and correspond to a less massive older star $M_\star = 1.48 \pm 0.06\ M_\odot$ (see Fig. 5). These solutions appear as the most probable due to the rapid evolution of stars at the end of the main sequence. We therefore adopted the post main-sequence solutions. While the mass for the two evolutionary phases differ by 14%, both sets of solutions give a radius that differs by less than 4% and thus have

[3] See the SciPy Web site at http://www.scipy.org

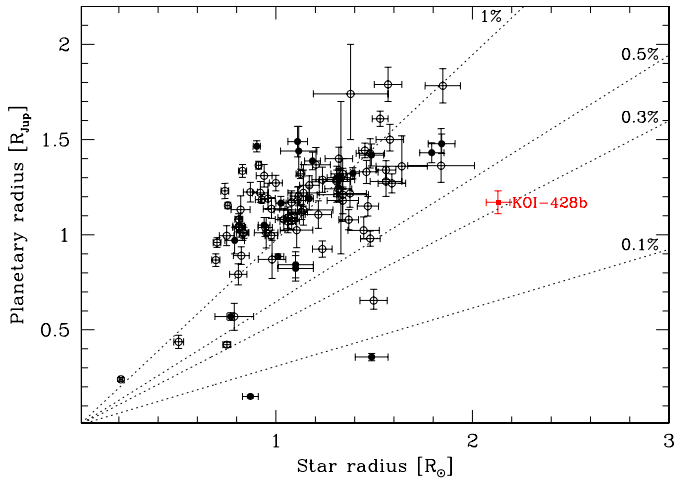

Fig. 6. Radius-radius diagram of all transiting exoplanets discovered so far, overplotted with curves of equal transit depth. Open circles show transiting planets discovered by ground-based photometry, filled circles are those discovered by space-based photometry, and the red square is KOI-428.

hardly any impact on the size of the planet. The inferred surface gravity is $\log g = 3.94 \pm 0.32$, in agreement with the spectroscopic value at 1-σ. Clearly a better estimate of the metallicity with a much higher quality spectrum would allow clearing out this uncertainty on the evolutionary status of the star and further on the mass. The stellar properties correspond to a spectral type F5IV. With the adopted stellar parameters, we derived $M_p = 2.2 \pm 0.4\, M_{\rm Jup}$ and $R_{\rm p} = 1.17 \pm 0.04\, R_{\rm Jup}$ for the transiting planet.

6. Discussion and conclusion

The hot Jupiter KOI-428b is the transiting planet with the largest host star detected so far ($2.13 \pm 0.06\, R_\odot$). Figure 6 shows the radius of transiting planets as a function of the radius of their host stars. Only five transiting planets orbit a star with a radius larger than 1.8 $R_\odot$ including Kepler-5 (Koch et al. 2010), Kepler-7 (Latham et al. 2010), TrES-4 (Mandushev et al. 2007), and HAT-P-7 (Pál et al. 2008). Transiting planets around such large stars are difficult to detect by ground-based photometry owing to the long transit duration and the small transit depth. We note that only eight candidates out of the 306 published in Borucki et al. (2010b) have an estimated host star radius larger than 1.8 $R_\odot$, including KOI-428.

From our determination of the stellar radius and the projected rotational speed of the star $\upsilon \sin i$, we note that the minimum star rotational period is $P_{\rm rot_{min}} = 11.9 \pm 2.7$ days, which is compatible with a synchronization at twice the planet orbital period. This is also the case for other transiting exoplanets (e.g. XO-4b, McCullough et al. 2008; HAT-P-6b, Noyes et al. 2008; HAT-P-8b, Latham et al. 2009) with host-star hotter than 6000 K (Lanza 2010). Additional photometry from *Kepler* might permit us to determine the true stellar rotational period (as for CoRoT-4b, Aigrain et al. 2008; Moutou et al. 2008) and then, help us to understand the star-planet interaction and evolution.

Planetary mass error bars are dominated by radial velocity uncertainties and stellar characterization uncertainties. Additional higher S/N spectra that permit better estimation of [Fe/H] and $T_{\rm eff}$ will definitely reduce the star mass uncertainties and the discrepancy between evolution solutions.

This detection demonstrates the efficiency of small telescopes with dedicated instrumentation for the ground-based follow-up of space missions like *Kepler* and *CoRoT* (Baglin et al. 2006). The equivalent of one night on a 2-m telescope led to establishing the planetary nature of a transiting candidate and to determining its mass. Only the follow-up of a significant amount of *Kepler* candidates will provide the real fraction of true transiting exoplanets.

Acknowledgements. We thank the technical team at the Observatoire de Haute-Provence for their support with the SOPHIE instrument and the 1.93-m telescope, and in particular, for the essential work of the night assistants. We are grateful to the *Kepler* Team for giving public access to the corrected *Kepler* light curve of Q1 data set and for publishing a list of good planetary candidates to follow-up. Financial support for the SOPHIE Consortium from the "Programme national de planétologie" (PNP) of CNRS/INSU, France and from the Swiss National Science Foundation (FNSRS) are gratefully acknowledged. We also acknowledge support from the French National Research Agency (ANR-08-JCJC-0102-01). A.E. is supported by a fellowship for advanced researchers from the Swiss National Science Foundation (grant PA00P2_126150/1). D.E. is supported by the Centre National d'Études Spatiales (CNES). R.F.D. would like to thank J.-M. Désert and A. S. Bonomo for fruitful discussions. A.S. would like to thank J.-C. Gazzano for all interesting discussions. The authors also thank the referee for his/her fruitful comments and suggestions.

References

Aigrain, S., Cameron, A. C., Ollivier, M., et al. 2008, A&A, 488, L43
Baglin, A., Auvergne, M., Boisnard, L., et al. 2006, 36th COSPAR Scientific Assembly, 36, 3749
Baranne, A., Queloz, D., Mayor, M., et al. 1996, A&AS, 119, 373
Barge, P., Baglin, A., Auvergne, M., et al. 2008, A&A, 482, L17
Batalha, N., Borucki, W., Bryson, S., et al. 2011, ApJ, in press
Bonomo, A. S., Santerne, A., Alonso, R., et al. 2010, A&A, 520, A65
Borucki, W. J., Koch, D. G., Brown, T. M., et al. 2010, ApJ, 713, L126
Borucki, W. J., & the Kepler Team 2010, ApJ, submitted [arXiv:1006.2799]
Bouchy, F., Hébrard, G., Udry, S., et al. 2009a, A&A, 505, 853
Bouchy, F., Moutou, C., Queloz, D., & the CoRoT Exoplanet Science Team 2009b, IAU Symp., 253, 129
Bruntt, H., Catala, C., Garrido, R., et al. 2002, A&A, 389, 345
Bruntt, H., De Cat, P., & Aerts, C. 2008, A&A, 478, 487
Bruntt, H., Deleuil, M., Frindlund, M., et al. 2010, A&A, 519, A51
Cardelli, J. A., Clayton, G. C., & Mathis, J. S. 1989, ApJ, 345, 245
Casagrande, L., Ramírez, I., Meléndez, J., Bessell, M., & Asplund, M. 2010, A&A, 512, A54
Dunham, E. W., Borucki, W. J., Koch, D. G., et al. 2010, ApJ, 713, L136
Gillon, M., Demory, B. O., Barman, T., et al. 2007, A&A, 471, L51
Jenkins, J. M., Borucki, W. J., Koch, D. G., et al. 2010, ApJ, 724, 1108
Jenkins, J. M., Caldwell, D. A., Chandrasekaran, H., et al. 2010, ApJ, 713, L87
Hébrard, G., Bouchy, F., Pont, F., et al. 2008, A&A, 488, 763
Holman, M. J., Fabrycky, D. C., Ragozzine, D., et al. 2010, Science, 330, 51
Kipping, D. M. 2010, MNRAS, 408, 1758
Kipping, D. M., & Bakos, G. Á. 2010, ApJ, submitted [arXiv:1004.3538]
Koch, D. G., Borucki, W. J., Rowe, J. F., et al. 2010, ApJ, 713, L131
Lanza, A. F. 2010, A&A, 512, A77
Latham, D. W., Bakos, G. Á., Torres, G.,et al. 2009, ApJ, 704, 1107
Latham, D. W., Borucki, W. J., Koch, D. G., et al. 2010, ApJ, 713, L140
Nelder, J. A., & Mead, R., 1965 Comput. J., 7, 308
Mandel, K., & Agol, E. 2002, ApJ, 580, L171
Mandushev, G., O'Donovan, F. T., Charbonneau, D., et al. 2007, ApJ, 667, L195
Moutou, C., Bruntt, H., Guillot, T., et al. 2008, A&A, 488, L47
McCullough, P. R., Burke, C. J., Valenti, J. A., et al. 2008, ApJ, submitted [arXiv:0805.2921]
Noyes, R. W., Bakos, G. Á., Torres, G., et al. 2008, ApJ, 673, L79
Pál, A., Bakos, G. Á., Torres, G., et al. 2008, ApJ, 680, 1450
Pepe, F., Mayor, M., Galland, et al. 2002, A&A, 388, 632
Perruchot, S., Kohler, D., Bouchy, F., et al. 2008, Proc. SPIE, 7014
Pollacco, D., Skillen, I., Cameron, A. C., et al. 2008, MNRAS, 385, 1576
Sing, D. K. 2010, A&A, 510, A21
Turck-Chièze, S., Palacios, A., Marques, J. P., & Nghiem, P. A. P. 2010, ApJ, 715, 1539